

# An M-Dwarf Stellar Companion in Cassiopeia and a Refinement on the Orbital Period for WASP-79b

J. A. ANDERSON  
University of St Andrews

January 26, 2023

## Abstract

*In this paper we describe the process by which TESS photometric data was analysed for the purpose of vetting a potential exoplanet candidate system and obtaining an improved orbital period for a known exoplanet. We present the first detailed reconnaissance of the J235028.76+504041.4 system and a refinement on the orbital period of the bloated Jupiter exoplanet WASP-79b. Analysis of TESS data for the J235028.76+504041.4 system strongly indicates the presence of a low-mass stellar companion in orbit with an F-class host star. This M-dwarf, henceforth referred to as J235028.76+504041.4b, was determined via transit fitting and MCMC analysis to have a radius  $3.82 \pm 0.24 R_{Jup}$  and an orbital period of  $1.778698 \pm 0.000036$  days. Transit timing of the known exoplanet WASP-79b was used to determine a more accurate orbital period than that reported by Smalley et al. in their 2012 discovery paper (Smalley et al. 2012). The improved orbital period of WASP-79b was found to be  $3.66231 \pm 0.00003$  days. We also present an estimate on the uncertainty of transit timing for WASP-79b twenty years from the current date as an example of the accuracy of projected future transits.*

## 1. INTRODUCTION

Transit photometry is a highly efficient method for detecting exoplanet candidates. The required observations can be made largely autonomously, with many stars being observed at any given time, and the methods by which these measurements are vetted for exoplanet candidates are becoming highly efficient as this field matures. TESS, or the Transiting Exoplanet Survey Satellite, is a joint MIT-NASA project whose primary mission was to monitor over 200,000 bright, nearby stars for the periodic dimming characteristic of a transiting exoplanet (Ricker, 2015). To meet its observation goals, TESS needed a position that was highly stable, had maximum sky coverage, and had a low radiation environment. The orbit selected was the P/2 High Earth Orbit - a previously unused 2:1 lunar resonance orbit. Compared to the more standard destination for large scale sky surveys, L2, this orbit would require less propellant to reach and would therefore allow for a lighter satellite (Gangestad, 2013). Exoplanet candidates are often revealed to be astrophysical false positives upon further analysis. The signal of a transiting planet can be mimicked by 1) a grazing stellar binary, 2) blended stellar binaries in the vicinity of a third bright star, or 3) a brown dwarf/M-star stellar companion (O'Donovan et al., 2006). The J235028.76+504041 system was observed by TESS in sectors 17, 24, and at the time of writing is currently being observed in sector 57. WASP-79b is a bloated

Jupiter discovered in 2012 using transit photometry and confirmed via radial velocity measurement (Smalley et al., 2012). B. Smalley et al. were able to identify a large range of stellar and planetary parameters, but did note that the radius was highly uncertain due to a lack of TRAPPIST photometry. A more recent paper by Addison et al. noted a significant spin/orbit misalignment with "the planet being in a nearly polar orbit" (Addison et al., 2013). The accuracy of measurement of this misalignment was later improved by Brown et al. who used WASP-79b to demonstrate various Rossiter-McLaughlin models (Brown et al., 2017). The planet was later observed in 2020 by TESS in sectors 4, 5, 31, and 32. Being able to accurately determine orbital parameters and their uncertainties is crucial in the study of exoplanets. Earth-like planets with large orbital periods, the search for which is considered a top priority in modern astronomy, can only be reliably observed when the uncertainty in that period is suitably low (Ford 2006).

## 2. TESS OBSERVATIONS

Information on the TESS mission described in this section was gathered primarily from a 2015 paper by Ricker et al. (Ricker et al., 2015). TESS data was gathered over a 600-1000nm bandpass - this being the greatest practical range for the proposed satellite design - using four identical CCD cameras each with a 24x24 degree FOV. A thirty minute cadence was used for observations during

the primary mission, but as of the time of writing of this paper TESS has resurveyed twenty six sectors with a ten minute cadence as part of its extended mission. The sector in which the known WASP exoplanet was observed falls into this category, meaning that there was a greater depth of data to work with, however the only available data for the J235028.76+504041.4 system was that with the thirty minute cadence. The bulk of stars observed reside in the F5-M5 spectral type due to their abundance and because previous photometry catalogues of these stars were often sparse. Stars were observed from a period ranging from one month to one year to allow for a wide range of maximum periods,  $P_{max}$ , and therefore open the possibility of detecting planetary systems more akin to our solar system. The TESS Input Catalogue, from which the data analysed in this report was gathered, is the result of TESS' primary mission and was created with the intent to "contain every optically luminous, persistent object in the sky" (Stassun, 2018).

### 3. ANALYSIS

Note: the processes detailed in this section apply to both the known WASP planet and the exoplanet candidate J235028.76+504041.4. Any difference in procedure has been identified in context of the section in which it occurred.

#### 3.1. Transit photometry

The first stage in the analysis of the TESS data was to generate a light curve and an orbital ephemeris. The TESS FFI data for the target was downloaded and then presented alongside a finding chart from the 2-Micron All-Sky Survey Catalogue to determine whether any nearby stars could be contaminating the signal.

Using this information, we were able to select appropriate photometry apertures the targets. For the known exoplanet host star WASP-79, there were few nearby stars and therefore a correspondingly low risk of background contamination. For the candidate star, a greater density of background stars were identified and therefore a careful selection of aperture size was required to minimise signal contamination. To determine the extent to which the target was blended with separate stellar sources, the centroid shifts during transit were analysed. Significant shifts in the observed centre of the light source could imply a blended binary system - a relatively common false positive for exoplanets (Cameron 2012). After verifying that alter-

**Figure 1:** TESS FFI data (left) and 2MASS finding chart (right) for WASP-79 (top) and J235028.76+504041.4 (bottom)

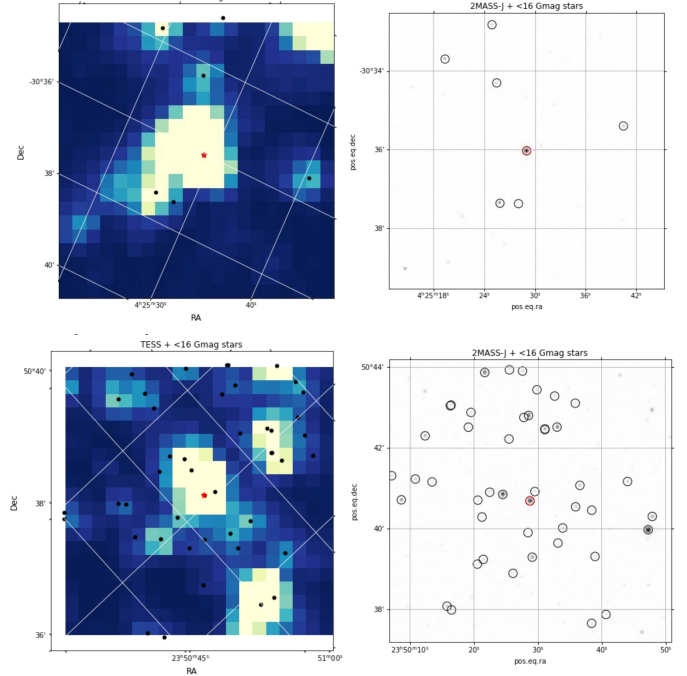
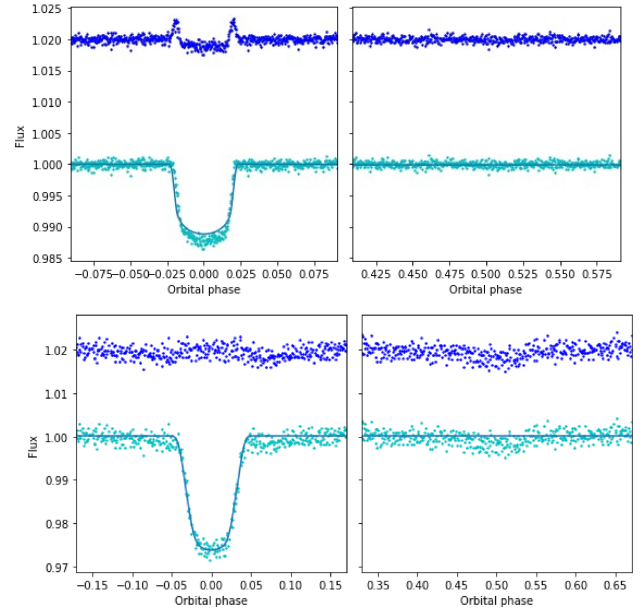


**Figure 2:** Transit light curves for WASP-79 (top) and J235028.76+504041.4 (bottom)



ations to aperture size did not visually reduce the centroid shifts, the raw light curve was extracted from the TESS data, plotted, and normalised to flatten it. This allowed us to isolate windows of poor data caused by instability in the TESS targeting (which occurred most drastically when TESS was at its closest approach to Earth). Once the light curve had been flattened and outlier data points removed, the period of the transit was determined using the Box Least-Squares algorithm. The BLS method assumes that the received signal has a well-defined period and searches for patterns that follow a square wave. This allows for highly efficient computation of the orbital period and ingress/egress duration by identifying statistically significant outliers to the square pattern (kovács et al., 2002). The crucial final step in this section of the analysis was to plot the light curve over twice the orbital phase and look for a secondary eclipse. The presence of a secondary eclipse does not entirely rule out the possibility of a target being an exoplanet - Jupiter-size bodies can have high enough reflectivity for the observed flux to dip when they pass behind a host star - but is a very strong indicator of an astrophysical false positive. WASP-79 showed no secondary eclipse as expected, but a faint secondary eclipse was observed for the J235028.76+504041 candidate. The ephemerides determined for WASP-79b and J235028.76+504041.4b respectively via the transit fitting in this section were

$$2459156.35695 + 3.66210E$$

$$2458969.19717 + 1.77821E$$

### 3.2. Spectro-photometric analysis

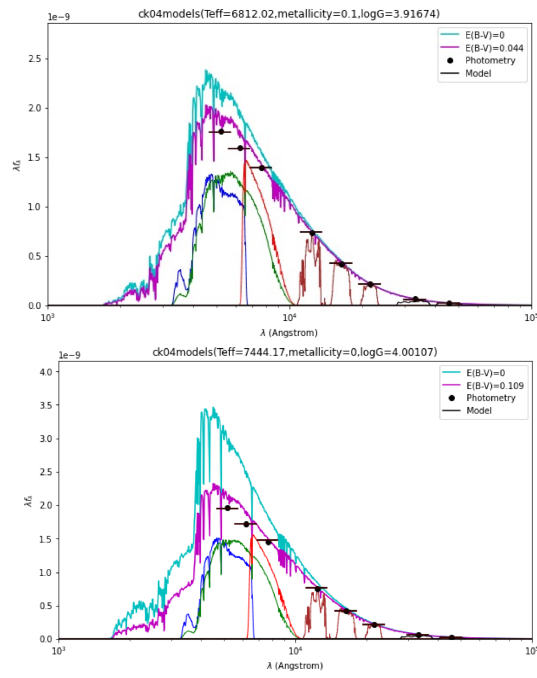
Having determined preliminary values for the orbital parameters, we could now utilise data from the Gaia, 2MASS and WISE catalogues to determine certain stellar parameters for our target systems. Using the Vizier Catalogue Service, we extracted bandpass values, apparent magnitudes, parallaxes, and reddening for our target systems. The first stellar parameter to be computed was the effective temperature,  $T_{eff}$ , which we determined by measuring the chi-squared fit to the observed data over a range of potential  $T_{eff}$ . The temperature which corresponded to the lowest chi-squared value was taken as the preliminary value. To determine stellar radius, we utilise the relation  $R/R_\odot = (T_\odot/T)^2(L/L_\odot)^{0.5}$ . The ratio of  $L/L_\odot$  is given by the ratios of apparent magnitude. The observed magnitude and a parallax from our target were listed in the Gaia data, and so we could determine the absolute magnitude of the target star. These values then allowed us

to determine the radius of the star in units  $R_\odot$ . These parameters were then used to fit a transit curve using the Python package PyCHEOPS, which we could then compare to the curve generated using the TESS photometry. This gave added assurance as to the presence (in the case of the J235028.76+504041.4 candidate) or absence (in the case of WASP-79) of a secondary transit. Once we had gathered good estimates on the relevant stellar parameters, we tested a model fit to the observed data using an MCMC procedure (described in the following section of the paper) to determine their uncertainties. The corner plot generated allowed us to get a rough estimate on the  $1 - \sigma$  uncertainty in stellar radius, which we determined by visual analysis to be  $0.05R_\odot$  for the J235028.76+504041.4 candidate and  $0.03R_\odot$  for WASP-79. These uncertainties are somewhat low for a spectrophotometric observation, but are not exceptional. Given the relatively high uncertainty in Gaia parallax, roughly 10% in the case of both the known and candidate exoplanet targets, it is likely that the uncertainty in stellar radius stems from this measurement more than it does from uncertainty in the photometry. With a sufficiently accurate transit fit and value for stellar radius, the radius of the transiting object could also be determined using the relation  $R_p = R_*\sqrt{\delta}$ , where  $\delta$  is the transit depth. Thus we were able to determine that the radii of the celestial bodies orbiting WASP-79 and J235028.76+504041.4 respectively were approximately  $1.32R_{Jup}$  and  $3.87R_{Jup}$ . Another important parameter now accessible to us was the orbital radius of the target bodies, which could be determined using the relation  $b = a\cos(i)/R_*$ .

### 3.3. Markov-Chain Monte Carlo analysis

To obtain the most accurate system parameters and their corresponding uncertainties, a full Markov-chain Monte Carlo analysis was performed using the priors determined by the previous transit and spectrophotometric fits. MCMC analysis is an efficient and versatile method for the fitting of a multi-parameter model to observed data, and for an accurate determination of the errors in those parameters. The procedure begins with prior estimated values for these parameters which are then perturbed in a random walk pattern, those values being periodically updated in real time to those determined by the MCMC procedure. This process is described in detail in a 2007 paper by Cameron et al. (Cameron et al. 2007), where the efficacy of the MCMC procedure is illustrated using SuperWASP data to identify exoplanet candidates for radial velocity follow-up. The first step in this stage of analysis

**Figure 3:** Spectral Energy Distributions for WASP-79 (top) and J235028.76+504041.4 (bottom)



was to define the functions that would calculate the so-called physical parameters from the state parameters of the system - those being mid-transit time, orbital period, impact parameter, transit depth and width, flux, parallax, stellar radius, and dust extinction. The initial priors used were selected from the earlier spectrophotometric analysis, then an initial "burn in" run and two tuning runs were completed to optimize the value by which each parameter would be perturbed in the final MCMC analysis. A step number of 100,000 was chosen for WASP-79, though technical constraints limited the step number to 10,000 for the analysis of J235028.76+504041.4. The result was a highly accurate set of physical parameters and corresponding uncertainties for the target systems, along with corner plots detailing the correlation between uncertainties. The Jupyter notebook used to generate these corner plots via the MCMC procedure was generously provided by A.C. Cameron of the University of St Andrews.

### 3.4. Transit timing analysis

Although the Box Least-Square method is known for its accuracy in determining orbital period, the mid-transit times of separate observations of a source often allow for an even more accurate value. We know that an integer

**Figure 4:** MCMC corner plots for WASP-79 (top) and J235028.76+504041.4 (bottom)

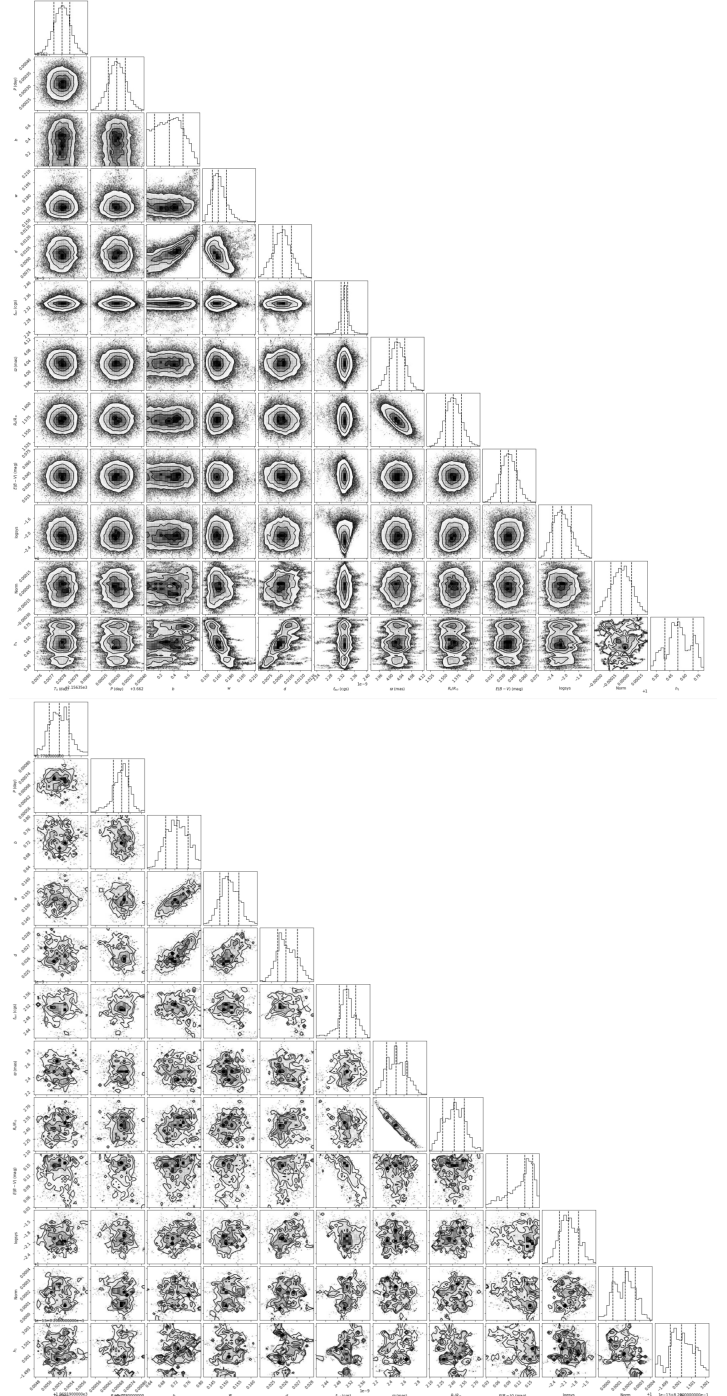


**Table 1:** Uncertainties regarding orbital period of WASP-79b

Parameter	Value
TESS mid-transit	2459256.35694
WASP mid-transit	2455545.235550
Time between observations	3611.12139d
Number of orbits	986
MCMC orbital period	3.66231d
Timing orbital period	3.66240d
Uncertainty in TESS mid-transit	0.00007d
Uncertainty in WASP mid-transit	0.00125d
Uncertainty in orbital period	0.0000051
Total uncertainty	0.001433d / 0.034hr

number of orbits must have elapsed between individual observations of a system, so by using the estimated orbital period determined by photometric analysis we are able to determine that orbit count. We can then take the elapsed time between observations and divide by that whole number to determine an improved orbital period. The BJD time of mid-transit for the TESS observation was 2459256.35694. The (converted) BJD time of mid transit from the initial discovery paper which utilised WASP photometry was 2455545.235550. Therefore the elapsed time between observations was 3611.12139 days. Dividing by the orbital period determined through MCMC analysis, we found the number of orbits in that period of time to be nine hundred and eighty six. Therefore, we were able to determine that the orbital period for WASP-79b is 3.662395 days. To determine the uncertainty in this measurement, the uncertainties in mid transit times and the uncertainty in estimated orbital period multiplied by the number of orbits were added in quadrature. Those uncertainties are described in table 1.

Using this data, we can predict the uncertainty in mid-transit time for WASP-79b twenty years from now. Twenty years is equivalent to 7403.84398 days, which means that given an orbital period of 3.66231 days the number of elapsed orbits of WASP-79b will be 1995 (rounded to the nearest whole orbit). To determine the uncertainty in the time at which this orbit will occur, we must multiply the uncertainty in orbital period by the number of elapsed orbits. This results in a value for the uncertainty in transit time twenty years in the future of 2.858 days.

#### 4. DISCUSSION

For both the known exoplanet WASP-79b and the J235028.76+504041.4b candidate, MCMC analysis showed

**Table 2:** System parameters of WASP-79b

Parameter	Value
Star	CD-30 1812
RA	4 <sup>hr</sup> 25 <sup>min</sup> 29.01 <sup>s</sup>
DEC	30° 36' 1.5"
Transit epoch (BJD, UTC), $T_0$	2459156.35780 ± 0.00007
Orbital period, $P$	3.66231 ± 0.00003d
Transit duration, $T$	0.16611 ± 0.00987
Transit depth, $(R_p / R_*)^2$	0.00951 ± 0.00128
Impact parameter, $b$	0.336 ± 0.217
Orbital inclination, $i$	87.3123 ± 0.1261°
Orbital eccentricity, $e$	0.008 ± 0.007
System parallax, $\pi$	4.026 ± 0.030mas
Stellar effective temperature, $T_{eff}$	6815 ± 50K
Stellar density, $\rho_*$	0.38 ± 0.09 $\rho_\odot$
Stellar mass, $M_*$	1.56 ± 0.38 $M_\odot$
Stellar radius, $R_*$	1.57 ± 0.02 $R_\odot$
Stellar surface gravity, $\log g_*$	4.240 ± 0.121
Planet radius, $R_p$	1.49 ± 0.10 $R_{Jup}$

**Table 3:** System parameters of J235028.76+504041.4b

Parameter	Value
Star	J235028.76+504041.4
RA	23 <sup>hr</sup> 50 <sup>min</sup> 28.76 <sup>s</sup>
DEC	50° 40' 41.4"
Transit epoch (BJD, UTC), $T_0$	2458969.19522 ± 0.00017
Orbital period, $P$	1.778698 ± 0.000036d
Transit duration, $T$	0.1515 ± 0.0033
Transit depth, $(R_p / R_*)^2$	0.2616 ± 0.0009
Impact parameter, $b$	0.727 ± 0.036
Orbital inclination, $i$	77.63 ± 0.31°
Orbital eccentricity, $e$	0.011 ± 0.010
System parallax, $\pi$	2.489 ± 0.158mas
Stellar effective temperature, $T_{eff}$	7615 ± 297K
Stellar density, $\rho_*$	0.16 ± 0.03 $\rho_\odot$
Stellar mass, $M_*$	2.03 ± 0.10 $M_\odot$
Stellar radius, $R_*$	2.42 ± 0.15 $R_\odot$
Stellar surface gravity, $\log g_*$	3.977 ± 0.033
Planet radius, $R_p$	3.82 ± 0.24 $R_{Jup}$

expected levels of correlation between the various orbital parameters determined. Impact parameter proved to be the variable with the greatest correlation to others as expected. The vast majority of other parameters appeared largely statistically independent, which adds to the reliability of the model transit created by the MCMC procedure.

The ephemerides determined for WASP-79b and J235028.76+504041.4b respectively were as follows:

$$2459156.35780 + 3.66231E$$

$$2458969.19522 + 1.778698E$$

Several methods were used to determine an updated orbital period for WASP-79b. First, transit timings from the original and TESS observations were used as follows. The time between observations was determined and then divided by the estimated orbital period to determine the number of orbits that had elapsed. Knowing this number must be an integer, it was rounded to the nearest whole number by which the elapsed time was then provided to give an accurate estimation of orbital period. This was determined to be 3.662395 days. However, MCMC analysis of the TESS data produced a value of 3.66231 days for the orbital period. This discrepancy is likely due to the uncertainties in mid-transit time for the two observations, and the relatively high uncertainty that arose from the propagation of orbital period uncertainty across the time period of the two observations. The transit timing result represents a slightly greater orbital period than that reported in the original discovery paper for WASP-79b, while the period determined by MCMC analysis was notably shorter. As the uncertainty in the value determined by the MCMC analysis has a significantly lower uncertainty than that determined by transit timing, that is the orbital period that was agreed upon as the most accurate. Accuracy is highly important in the analysis of exoplanets, particularly for those with large orbital periods in which transits are few and far between. Markov-chain Monte Carlo analysis has proven a valuable tool for determining a wide range of stellar and planetary parameters and will remain highly relevant in the field of exoplanet observation.

The elimination process by which the J235028.76+504041.4 exoplanet candidate was determined to be a low-mass stellar companion is described by Schanche et al. in their 2019 paper (Schanche et al. 2019). Based on their guidelines, data collected from analysis of the J235028.76+504041.4 system shows strong evidence of an F-class/M-dwarf stellar companion system. A lack of notable centroid shifts limits the probability of this system being a blended binary (Schanche et al.,

2019) and the clear presence of a U-shaped transit curve largely rules out the possibility of an eclipsing binary (Santerne et al., 2015). The stellar properties determined by spectrophotometric analysis are unexceptional, which means there is little cause to believe that this signal could be the result of astroseismological effects (Schance et al., 2021). However, the presence of a dim secondary eclipse alongside the large radius of the orbiting body make it exceedingly unlikely that it is in fact an exoplanet. A radius of  $3.82 R_{Jup}$  puts this celestial body firmly in the region of M-dwarfs, and so it is the final decision of this report to suggest this as the nature of the J235028.76+504041.4 system. Relatively few M-dwarfs have been well observed to date, despite them being the most populous class of star in our local region (Eigmüller et al., 2011). A more detailed catalogue of such stars would prove useful in furthering our understanding of the stellar population of our galaxy. One pressing issue in the study of low mass stars is the so-called radius discrepancy - a persisting deviation between the observed and predicted radii of low mass stars. This discrepancy is most acute when considering binary systems with short orbital periods (Spada et al, 2013). As such, we firmly believe that this result merits a more detailed analysis of the J235028.76+504041.4 system.

## REFERENCES

- (Addison et al., 2013) Addison, B. C., et al., 2013, AJL 774, L9
- (Brown et al., 2017) Brown, D. J. A., et al., 2017, MN-RAS 464:810-839
- (Cameron, et al., 2007) Cameron, A. C., et al., 2007, MNRAS 380:1230-1244
- (Cameron, 2012) Cameron, A. C., 2012, Nature 492:48-50
- (Eigmüller et al., 2011) Eigmüller, P., et al., 2011, AJ 151 84
- (Ford, 2006) Ford, E. B., 2006, AJ 642:505-522
- (Gangestad et al., 2013) Gangestad, J. W., et al., 2013, Astrodynamics 150:1585-1604
- (Kováks et al., 2002) Kováks, G., Zucker, S., Mazeh, T., 2002, AA 391:369-377
- (O'Donovan et al., 2004) O'Donovan, F. T., et al., 2006, AIP Conference Proceedings 713:151-160
- (Ricker et al., 2015) Ricker, G. R., et al., 2015, JATIS 1, 014003
- (Santerne et al., 2013) Santerne, A., et al., 2013, AA 557 A139
- (Schanche et al., 2019) Schanche, N., et al., 2019, MN-RAS 488, 4905
- (Schanche et al., 2021) Schanche, N., et al., Unpublished PLATO WP113-100 mission technical document, communicated by AC Cameron
- (Smalley et al., 2012) Smalley, B., et al., 2012, AA 547, A61
- (Spada et al., 2013) Spada, F., et al., 2013, ApJ 776:87
- (Stassun et al., 2018) Stassun, K. G., et al., 2018, AJ 156, 102